The Kinematic Bicycle Model: a Consistent Model for Planning Feasible Trajectories for Autonomous Vehicles?

Philip Polack[1], Florent Altché[1,2], Brigitte d'Andréa-Novel[1] and Arnaud de La Fortelle[1]

Abstract— Most autonomous driving architectures separate planning and control phases in different layers, even though both problems are intrinsically related. Due to limitations on the available computational power, their levels of abstraction and modeling differ; in particular, vehicle dynamics are often highly simplified at the planning phase, which may lead to inconsistency between the two layers. In this paper, we study the kinematic bicycle model, which is often used for trajectory planning, and compare its results to a 9 degrees of freedom model. Modeling errors and limitations of the kinematic bicycle model are highlighted. Lastly, this paper proposes a simple and efficient consistency criterion in order to validate the use of this model for planning purposes.

I. INTRODUCTION

Research on autonomous vehicles has mainly focused on three main layers: perception, planning and control. Each one of these layers presents very different specificities, and are often addressed separately, with in general strong assumptions on the behavior of the other components of the vehicle.

In this article, we focus on the link between trajectory planning and low-level control. In many studies (see, *e.g.*, [1], [2]), the low-level control is not considered at the motion planning phase; instead, the general assumption is that, provided the planned trajectory satisfies a certain set of constraints, the low-level control will be able to track this trajectory with a bounded error. In some actual implementations [3], the low-level controller is provided by the test car OEM as a black-box, with hard limits on the acceptable inputs of this control to prevent the vehicle from leaving its handling envelope. Such "black-box" behavior effectively fully isolates motion planning and control.

Conversely, research on low-level vehicle control often assumes that a predefined reference trajectory is known in advance and does not change over time. Due to the presence of mobile obstacles on the road, notably other traffic participants, this assumption is in general untrue. Interestingly, motion planning and control for autonomous vehicles often rely on relatively similar techniques, and namely Model Predictive Control (MPC). This method uses a model of the vehicle dynamics to find a sequence of feasible control inputs minimizing a given cost function, and has been used for multiple applications, for instance to control a vehicle near its handling limits [4], [5] or plan overtaking trajectories [6]. However, motion planning considers time scales up to several seconds, whereas low-level control generally focuses on sub-second horizons. Moreover, motion planning problems need much more computational cost in order to be solved. Therefore, and even though the two problems can be treated using MPC, the vehicle models used are widely different.

The 3 degrees of freedom kinematic bicycle model is one of the simplest models frequently used at the motion planning phase, with the belief that it is able to capture enough of the nonholonomic constraints of the actual vehicle dynamics. By contrast, even relatively simple vehicle models used for low-level control can imply more than 10 degrees of freedom. However, relatively little research has been performed on the adequacy of the model used for motion planning with the actual vehicle control. Reference [7] compared the results from a 2 degrees of freedom dynamic bicycle model for planning and a precise, 14 degrees of freedom vehicle model with satisfying results, but the study is only focused on driving far from the handling limits of the vehicle. Reference [8] compared the predictive power of an MPC planner based on the kinematic bicycle model and a planner using a linear dynamic bicycle model, and concluded that the kinematic model performs satisfactorily. However, no simple criterion for checking the validity of the kinematic bicycle model has been proposed. Therefore, this paper proposes to underline the differences between motion planning and control problems. It compares the kinematic bicycle model with a very accurate 9 Degrees of Freedom (9DoF) one, and gives a practical bound where both models coincide so that consistency checking can be made quickly.

The rest of this paper is organized as follows: Sections II and III respectively summarize the motion planning and the control problems, underlying the specificity of each. Section IV presents the vehicle and tire models used for simulations. Section V compares the kinematic bicycle model with the 9DoF model. Lastly, Section VI concludes this paper.

II. MOTION PLANNING

A. The motion planning problem

In [9], the author has shown that any admissible motion of a three-dimensional mechanical system appears as a collision-free path for a point in the Configuration Space *CS*, i.e. the space of all the possible configurations of the system.

Problem 1 – Given an initial configuration q_{init}, a goal region configuration CS_{goal} and some constraint functions h, the motion planning problem consists in finding a feasible trajectory $w : [0,T] \rightarrow CS_{free}$ such that $w(0) = q_{init}$, $w(T) \in CS_{goal}$, satisfying all the constraints imposed by h.

CS_{free} refers to the free configuration space, namely the region such that if $q \in CS_{free}$, the vehicle does not hit any obstacles.

If a solution exists, the number of feasible trajectories is infinite. Therefore, the problem can be augmented to an optimal control problem to choose the best feasible trajectory:

Problem 2 – Given an initial configuration q_{init}, a goal region CS_{goal}, some constraint functions h and a cost function J, the optimal motion planning problem consists in finding an optimal feasible trajectory $w^* : [0,T] \rightarrow CS_{free}$ such that $w^*(0) = q_{init}$, $w^*(T) \in CS_{goal}$, respecting all the constraints h and with w^* minimizing the cost function, i.e.:

$$J(w^*) = \min_{w \in W_{feasible}} J(w) \tag{1}$$

In the case of autonomous vehicle, we have two main categories of constraints: avoiding obstacles and respecting the vehicle's dynamics. The former corresponds to avoiding forbidden regions of the configuration space (the complementary of CS_{free}). The latter corresponds to the admissible motions for the vehicle in the configuration space. In particular, cars have nonholonomic dynamic constraints (see [10]), as they cannot move laterally without a longitudinal movement.

B. Levels of Abstraction

In the motion planning problem, an obstacle is usually considered as a region of the configuration space including uncertainty on its exact position and a safety margin. Moreover, moving obstacles are usually assumed to keep a constant speed during the numerical resolution of the motion planning (see [6]).

C. Solutions

The motion planning problem, also referred to the "piano-mover" problem has been proven to be decidable [11] and PSPACE-hard [12]. The complexity of analytical solutions makes them unsuitable for real time application. Therefore, numerical approximation methods are used. They rely either on sampling of the configuration (or control) space, or on constrained optimization techniques such as MPC. Among sampling methods, stochastic sampling (for instance Rapid-exploring Random Tree - RRT - algorithms) are often preferred over deterministic sampling due to the high dimensionality of the space. A full review on Motion Planning techniques can be found in [13] and [14].

D. Vehicle Behavior Modeling

In all cases, the behavior of the vehicle needs to be modeled to find feasible motions.

- For RRT, Dubins' path [15] or Reeds and Shepp's path [16] are often used such as in [17].

- For MPC, the kinematic bicycle model presented in next section is very popular (see for example [2], [18] and [19]).

E. MPC using a kinematic bicycle model

In the rest of the paper, we will focus on planning with MPC using a kinematic bicycle model.

In the kinematic bicycle model, the two front wheels (resp. the two rear wheels) of the vehicle are lumped into a unique wheel located at the center of the front axle (resp. of the rear axle) such as illustrated on Figure 1. The control inputs correspond to the acceleration u_1 and the front wheel steering angle u_2 of the vehicle, when assuming that only the front wheel can be steered. The kinematic bicycle model can then be written [20] as:

$$\dot{X} = V \cos(\psi + \beta(u_2)) \tag{2a}$$
$$\dot{Y} = V \sin(\psi + \beta(u_2)) \tag{2b}$$
$$\dot{V} = u_1 \tag{2c}$$
$$\dot{\psi} = \frac{V}{l_r} \sin(\beta(u_2)) \tag{2d}$$

where $\beta(u_2)$ is the slip angle at the center of gravity:

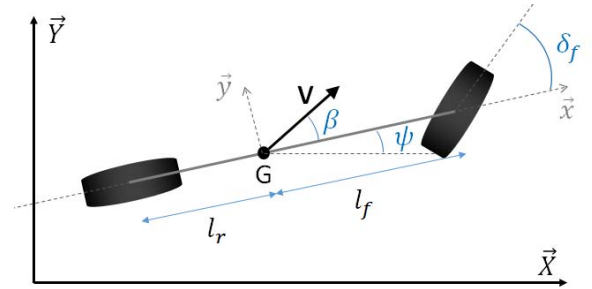$$\beta(u_2) = \arctan\left(\tan(u_2)\frac{l_r}{l_f + l_r}\right) \tag{2e}$$

Fig. 1.   Kinematic bicycle model of the vehicle

III. LOW-LEVEL CONTROL

A. The control problem

Problem 3 – Given a list of waypoints $(w_i)_{i \in I} = (X_i, Y_i, V_i)_{i \in I}$, where (X_i, Y_i) are the successive reference positions of the vehicle in the ground frame and V_i the successive speed references at position (X_i, Y_i), the control problem consists in finding a sequence of feasible control inputs $(u_i)_{i \in I}$ that stabilizes the system and tracks the reference trajectory given by the waypoints.

Other additional criteria can be taken into account such as the time response of the system, driving comfort or energy consumption.

B. Levels of Abstraction

In the low-level control part, the obstacles are usually not considered: the reference trajectory given by the motion planner is assumed to be collision-free within a certain margin. Therefore, the consistency between the two layers

is critical for the safety of the vehicle: a trajectory that is unfeasible or too difficult to follow for the controller might lead to a crash, as illustrated on Figure 2. In this example, the planned trajectory avoids colliding with the rear yellow vehicle; however, due to the actual vehicle dynamics, the best feasible trajectory is shown in red (dashed). Moreover, due to control errors, the trajectory actually followed by the vehicle is the yellow one, which would result in a collision.
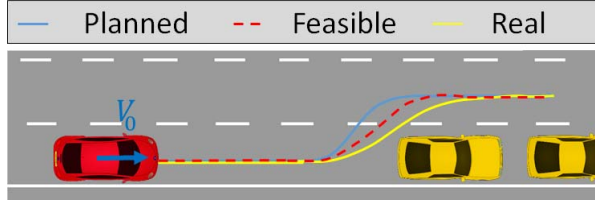

Fig. 2. Consistency between motion planning, low-level control and real trajectory

C. Solutions

1) Kinematic-based controllers: These controllers are based on the geometry and on the speed of the vehicles as in Equation (2). They assume no slip and no skip. Therefore, they are usually limited to low-speed application. Among them, we can mention [20], [21] and [22].

2) Dynamic-based controllers: These controllers are based on the 3 Degrees of Freedom (3DoF) dynamic bicycle model of the vehicle presented in Equations (3) combined with a linear tire model (see Equation (4)). The notations are summarized in Table I.

$$m(\dot{V}_x - \dot{\psi}V_y) = F_{xf} + F_{xr} \quad \text{(3a)}$$
$$m(\dot{V}_y + \dot{\psi}V_x) = F_{yf} + F_{yr} \quad \text{(3b)}$$
$$I_z\ddot{\psi} = l_f F_{yf} - l_r F_{yr} \quad \text{(3c)}$$

The subscripts f and r correspond respectively to the front and rear wheel of the bicycle model.

$$F_{xp_f} = C_{\tau_f}\tau_{x_f} \qquad F_{yp_f} = C_{\alpha_f}\left(\delta_f - \frac{V_y + l_f\dot{\psi}}{V_x}\right) \quad \text{(4a)}$$

$$F_{xp_r} = C_{\tau_r}\tau_{x_r} \qquad F_{yp_r} = -C_{\alpha_r}\left(\frac{V_y - l_r\dot{\psi}}{V_x}\right) \quad \text{(4b)}$$

C_τ (resp. C_α) corresponds to the longitudinal (resp. lateral) tire stiffness coefficient.

One method consists in considering V_x as a parameter of Equations (3b) and (3c) to get a Linear Parameter Varying (LPV) system such as done in [20]. Another solution is to use the flatness property of the 3DoF model (see [23] and [24]).

3) Model Predictive Control (MPC): Model Predictive Control approaches are quite popular to deal with some more accurate modeling of the vehicle, especially to consider more complex tire models such as done in [25], [26], [27] or [5]. In this case, the model is used to predict the future states of the vehicle. An optimisation algorithm computes the optimal control input to be applied to the system.

4) Model-free Control: At last, controllers based on correcting the tracking error with no modeling of the system such as the popular Proportional-Integral-Derivative (PID) controller [28] or the recently introduced Model-free Control [29] can be used to control the vehicles.

IV. SIMULATION MODEL

In this section, we describe the 9 Degrees of Freedom (9DoF) vehicle model used in order to simulate the dynamic of the vehicle. They correspond to 3DoF for the whole vehicle ($V_x, V_y, \dot{\psi}$), 2DoF for the car body ($\dot{\theta}, \dot{\phi}$) and 4DoF for the wheels ($\omega_{fl}, \omega_{fr}, \omega_{rl}, \omega_{rr}$). The model takes into account both the coupling of longitudinal and lateral slips and the load transfer between tires. The control inputs of the simulator are the torques T_{ω_i} applied at each wheel i and the steering angle of the front wheel δ_f. The low-level dynamics of the engine and brakes are not considered here. The notations are given in Table I and illustrated in Figure 3.

Remark: the subscript $i = 1..4$ refers to each of the four wheels of the vehicle in the following order: front left (fl), front right (fr), rear left (rl) and rear right (rr).

TABLE I
NOTATIONS

|	
X, Y	Position of the center of gravity of the vehicle in the ground framework
θ, ϕ, ψ	Roll, pitch and yaw angles of the car body
V_x, V_y	Longitudinal and lateral speed of the vehicle in its inertial frame
V_{xp_i}	Longitudinal speed of the center of rotation of wheel i expressed in the tire frame
ω_i	Angular velocity of the wheel i
I_x, I_y, I_z	Inertia of the vehicle around its roll, pitch and yaw angles
I_{r_i}	Inertia of the wheel i
T_{ω_i}	Total torque applied to the wheel i
F_{xp_i}, F_{yp_i}	Longitudinal and lateral tire forces expressed in the tire frame
F_{x_i}, F_{y_i}	Longitudinal and lateral tire forces expressed in the vehicle frame
F_{z_i}	Normal reaction forces on wheel i
M_T	Total mass of the vehicle
l_f, l_r	Distance between the front (resp. rear) axle and the center of gravity
l_w	Half-track of the vehicle
h	Heigth of the center of gravity
r_{eff}	Effective radius of the wheel
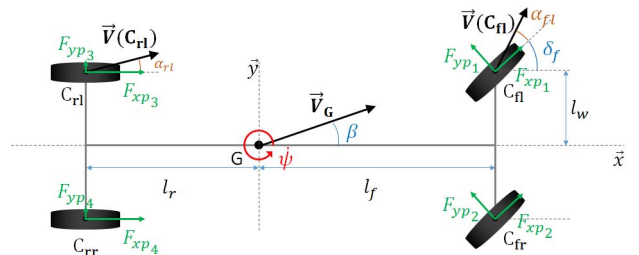
Fig. 3. Simulation model of the vehicle

Several simplifying assumptions were made during the modeling:

- Only the front wheels are steerable.
- The roll and pitch rotations happen around the center of gravity.
- The aerodynamic force is applied at the heigth of the center of gravity. Therefore, it does not involve any moment on the vehicle.
- The slope and road-bank angle of the road are not taken into account which is a usual assumption.

A. Vehicle model

The dynamics of the longitudinal, lateral and yaw motions of the whole vehicle are given by the following Equations:

$$M_T \dot{V}_x = M_T \dot{\psi} V_y + \sum_{i=1}^{4} F_{x_i} - F_{aero} \tag{5a}$$

$$M_T \dot{V}_y = -M_T \dot{\psi} V_x + \sum_{i=1}^{4} F_{y_i} \tag{5b}$$

$$I_z \ddot{\psi} = l_f(F_{y_1} + F_{y_2}) - l_r(F_{y_3} + F_{y_4}) \\ + l_w(F_{x_2} + F_{x_4} - F_{x_1} - F_{x_3}) \tag{5c}$$

where F_{x_i} and F_{y_i} are respectively the longitudinal and lateral tire forces generated by the road on wheel i in the vehicle frame.

The position (X, Y) of the vehicle in the ground framework is given by the following Equations:

$$\dot{X} = V_x \cos \psi - V_y \sin \psi \tag{5d}$$

$$\dot{Y} = V_x \sin \psi + V_y \cos \psi \tag{5e}$$

B. Car body model

The dynamics of the roll and pitch motion of the car body are given by the following Equations:

$$I_x \ddot{\theta} = l_w(F_{z_1} + F_{z_3} - F_{z_2} - F_{z_4}) + h \sum_{i=1}^{4} F_{y_i} \tag{5f}$$

$$I_y \ddot{\phi} = l_r(F_{z_3} + F_{z_4}) - l_f(F_{z_1} + F_{z_2}) - h \sum_{i=1}^{4} F_{x_i} \tag{5g}$$

where F_{z_i} are damped mass/spring forces depending on the suspension travel ζ_i due to the roll θ and pitch ϕ angles:

$$F_{z_i} = -k_s \zeta_i(\theta, \phi) - d_s \dot{\zeta}_i(\theta, \phi) \tag{5h}$$

where k_s and d_s are respectively the stiffness and the damping coefficients of the suspension.

C. Wheel dynamics

The dynamics of each wheel $i = 1..4$ expressed in the tire frame is given by the following Equation:

$$I_r \dot{\omega}_i = T_{\omega_i} - r_{eff} F_{xp_i} \tag{5i}$$

D. Tire Dynamics

The longitudinal force F_{xp_i} and the lateral force F_{yp_i} applied by the road on each tire i are functions of the longitudinal slip ratio τ_{x_i}, the side-slip angle α_i, the reactive normal force F_{z_i} and the road friction coefficient μ:

$$F_{xp_i} = f_x(\tau_{x_i}, \alpha_i, F_{z_i}, \mu) \tag{6a}$$

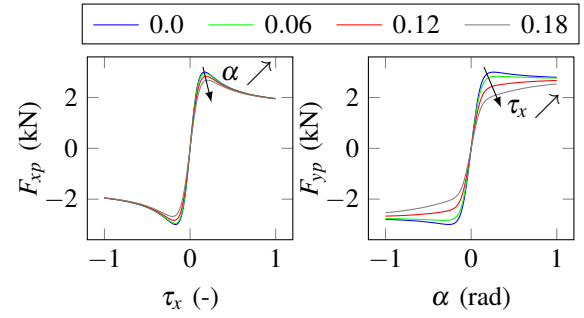$$F_{yp_i} = f_y(\alpha_i, \tau_{x_i}, F_{z_i}, \mu) \tag{6b}$$

Fig. 4. Impact of combined slip tire model on force generation: the abscissa represents the slip parameter mainly responsible for force generation and the colored lines represents different values of the other slip parameter
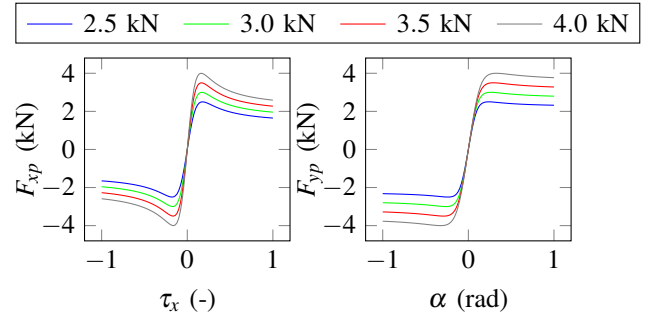

Fig. 5. Impact of normal forces F_z on tire force generation for a nominal load of 3kN

The longitudinal slip ratio of the wheel i is defined as following:

$$\tau_{x_i} = \begin{cases} \frac{r_{eff} \omega_i - V_{xp_i}}{r_{eff} \omega_i} & \text{if } r_{eff} \omega_i \geq V_{xp_i} \text{ (traction)} \\ \frac{r_{eff} \omega_i - V_{xp_i}}{|V_{xp_i}|} & \text{if } r_{eff} \omega_i < V_{xp_i} \text{ (braking)} \end{cases} \tag{7}$$

The lateral slip-angle α_i of tire i is the angle between the direction given by the orientation of the wheel and the direction of the velocity of the wheel:

$$\alpha_f = \delta_f - \text{atan}\left(\frac{V_y + l_f \dot{\psi}}{V_x \pm l_w \dot{\psi}}\right); \; \alpha_r = -\text{atan}\left(\frac{V_y - l_r \dot{\psi}}{V_x \pm l_w \dot{\psi}}\right) \tag{8}$$

In order to model the functions f_x and f_y, we used the combined slip tire model presented by Pacejka in [30] (Equations (4.E1) to (4.E67)) which takes into account the interaction between longitudinal and lateral slips on the force generation as illustrated on Figure 4. Therefore, the friction circle due to the laws of friction $||\vec{F}_{xp} + \vec{F}_{yp}|| \leq \mu ||\vec{F}_z||$ is respected. The impact of load transfer between tires is also taken into account through F_z and is illustrated on Figure 5.

Lastly, the relation between the tire forces expressed in the vehicle framework F_x and F_y and the ones expressed in the tire framework F_{xp} and F_{yp} is given in Equation (9):

$$F_{x_i} = (F_{xp_i} \cos \delta_i - F_{yp_i} \sin \delta_i) \cos \phi - F_{z_i} \sin \phi \tag{9a}$$

$$F_{y_i} = (F_{xp_i} \cos \delta_i - F_{yp_i} \sin \delta_i) \sin \theta \sin \phi \\ + (F_{yp_i} \cos \delta_i + F_{xp_i} \sin \delta_i) \cos \theta + F_{z_i} \sin \theta \cos \phi \tag{9b}$$

V. RESULTS

In order to evaluate the consistency of using a kinematic bicycle model for trajectory planning purpose, we compared the model with the one presented in Section IV. Circles with different radius R travelled at constant speed V were chosen as reference trajectories because they correspond to constant control inputs for the kinematic model: $u_1 = 0$ and $u_2 = \delta_{th}$.

The position of the vehicle given by a kinematic bicycle model is then the following:

$$X(t) = R\sin(\psi(t) + \beta) + X(0) \tag{10a}$$
$$Y(t) = -R\cos(\psi(t) + \beta) + Y(0) \tag{10b}$$
$$\psi(t) = \frac{V}{R}t + \psi(0) \tag{10c}$$

As $\dot{\psi} = V/R$ is constant, we get from Equations (2d) and (2e) that δ_{th} is a function only of radius R, given by Equation (11):

$$\delta_{th}(R) = \arctan\left(\left(\frac{l_f}{l_r} + 1\right)\tan\left(\arcsin\left(\frac{l_r}{R}\right)\right)\right) \tag{11}$$

Note that in the kinematic controller, R does not depend on the speed V, but only on the value of $u_2 = \delta$ as shown in Equation (11).

The value of the different main parameters are the following: $l_f = 1.17$m, $l_r = 1.77$m, $l_w = 0.81$m, $M_T = 1820$kg and $\mu = 1$.

A. Kinematic bicycle model without bounds

In this section, we are going to test the constant radius assumption of the kinematic model for a given steering angle δ on the simulation model presented in Section IV. For that purpose, we have run several simulations parameterized by different constant steering angles δ, an initial speed $V_x = 10$m/s and successive wheel torque commands T_ω applied at the front wheels. The system ends up describing a circle with constant speed (see Figures 6 and 7), except if the wheel torques are negative or too high. These solutions were discarded. The radius R of the circle versus speed V is displayed on Figure 8 for different values of the applied steering angle.
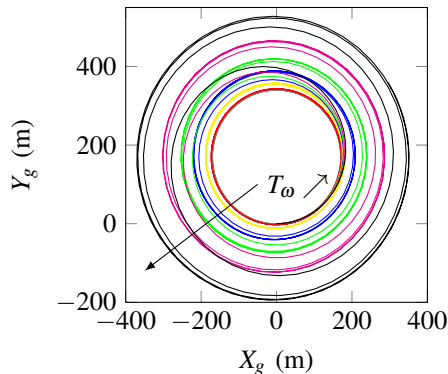

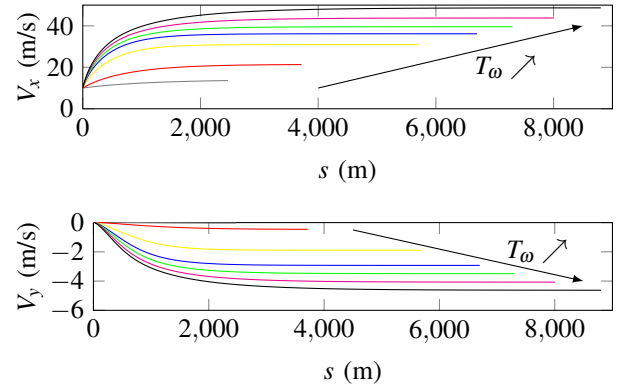Fig. 6. Exemple of trajectories obtained with $\delta_f = 1°$ for different applied wheel torques T_ω

Fig. 7. Exemple of speed profiles obtained with $\delta_f = 1°$ for different applied wheel torques T_ω. The colors matches with the trajectories of Figure 6
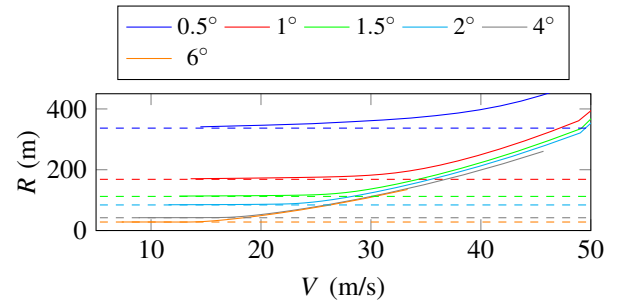

Fig. 8. Radius versus speed for different steering angles obtained with the 9DoF model (full lines) and the kinematic bicycle model (dashed lines)

We observe that the constant radius assumption is false, especially as V or δ increases. The error on the radius is increasing very fast: at $V = 25$m/s, the error is 4.0% for $\delta = 1°$ and 86.0% for $\delta = 4°$.

From the results above, we obtained for a given applied steering angle δ_a in the simulator a curve $R = f(V)$. Moreover, we know that for a given R corresponds a theoretical δ_{th} obtained from the kinematic bicycle model and given by Equation (11). Therefore, we have plotted in Figure 9 the theoretical steering angle δ_{th} corresponding to the radius R obtained above. At low-speed, we observe that δ_a and δ_{th} are equal. However, at higher speeds, δ_{th} decreases rapidly, except at low steering angle δ_a. Thus, on the simulation model, the vehicle is understeering compared to the kinematic model at high speed. This is due to slip. Therefore, the kinematic bicycle model is a good modeling for low-speed vehicles but seems to not be precise enough for vehicles at high speed. Using it for planning purpose might lead to completely unfeasible trajectories for the vehicle.

B. Taking into account the lateral acceleration

The lateral acceleration a_y of the vehicle can be expressed as a function of its speed V and the curvature radius R as:

$$a_y = \frac{V^2}{R} \tag{12}$$

Therefore, we computed a_y for the different values of V and R obtained on Figure 8. The results are shown in
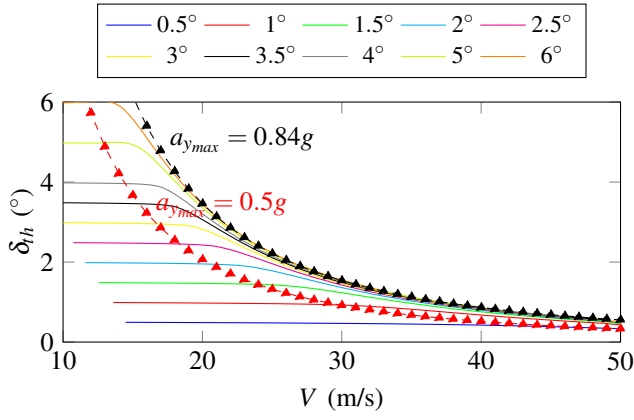
Fig. 9. Theoretical kinematic steering angle δ_{th} obtained by applying a steering angle δ_a on the 9DoF model (full line), and maximum kinematic steering angle δ_{max} allowed for different maximum lateral accelerations $a_{y_{max}}$ (triangles)

Figure 10. We observe that the lateral acceleration obtained by the simulator is saturated by $a_{y_{max}} = 8.22 \text{m/s}^2 = 0.84g$ at high speeds and non-small steering angles.
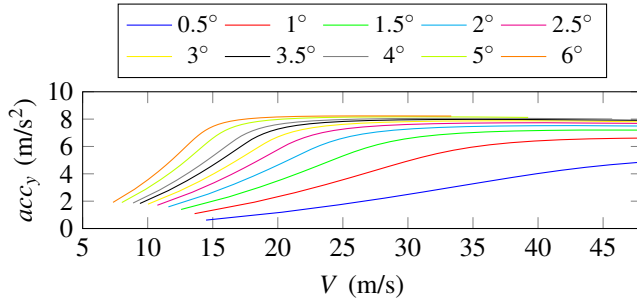

Fig. 10. Lateral acceleration versus speed for different steering angles obtained with the simulation model

Moreover, given a maximum allowed lateral acceleration $a_{y_{max}}$ for the vehicle, we can compute a maximum allowed steering angle δ_{max} given by the kinematic bicycle model for each V:

$$\delta_{max} = \arctan\left(\left(\frac{l_f}{l_r} + 1\right)\tan\left(\arcsin\left(\frac{a_{y_{max}} l_r}{V^2}\right)\right)\right) \quad (13)$$

The dotted lines of Figure 9 show the curve δ_{max} versus speed V for different values of $a_{y_{max}}$. By taking the value $a_{y_{max}} = 8.22 \text{m/s}^2$, we obtain the maximum steering enabled at a given speed. We also observe that $a_y \leq 0.5g$ seems a good limitation of the validity of the kinematic bicycle model.

Therefore, using a kinematic bicycle model with a limitation on the lateral acceleration at around $0.5g$ or less gives good results, generating feasible path for the low-level controller. Above this limit, the model is unable to generate a feasible track and should be avoided. More accurate models including the vehicle dynamics should in this case be used.

C. The dry road assumption

We run the same simulations as before but this time with $\mu = 0.7$ corresponding to a wet road. The results are shown

on Figure 11 and 12. We observe again the importance of limiting the lateral acceleration of the vehicle in order for the kinematic controller to be valid, but this time at an empiric value of $a_{y_{max}} = 0.5\mu g$.
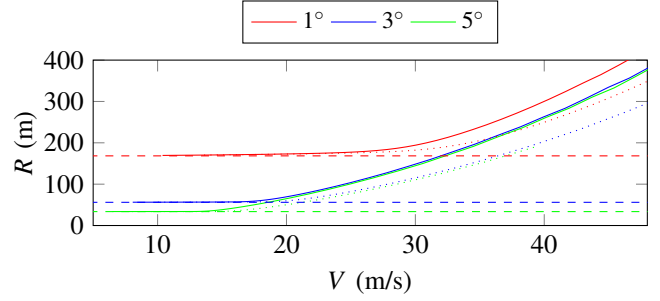

Fig. 11. Radius versus speed for different steering angles obtained with the 9DoF model for $\mu = 0.7$ (full lines), $\mu = 1$ (dotted lines) and with the kinematic bicycle model (dashed lines)
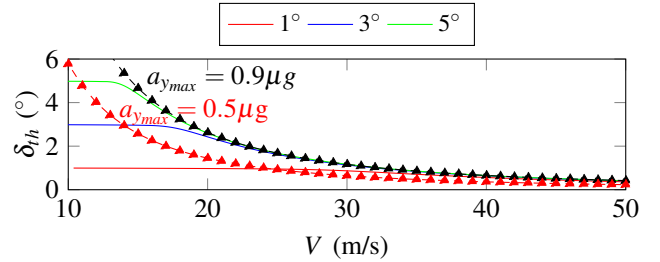

Fig. 12. Theoretical kinematic steering angle δ_{th} obtained by applying a steering angle δ_a on the 9DoF model with $\mu = 0.7$ (full line), and maximum kinematic steering angle δ_{max} allowed for different maximum lateral accelerations $a_{y_{max}}$ (triangles)

VI. CONCLUSIONS

We have studied the consistency of using a kinematic bicycle model for trajectory planning purposes by comparing its results with those provided by a complex realistic vehicle model. The results showed the importance of limiting the lateral acceleration a_y of the vehicle to a value lower than $0.5\mu g$. In this case, using a kinematic bicycle model for motion planning purposes seems consistent, generating a feasible trajectory for the low-level controller. However, the model errors can become very large when the constraint on lateral acceleration is not respected. Therefore, a more accurate vehicle model should be used when dealing with higher accelerations to push the vehicle's dynamics near its handling limits.

Future work will focus on using this simple and efficient consistency check criterion together with a Model Predictive Control based on a kinematic bicycle model for further validation.

REFERENCES

[1] W. Zhan, C. Liu, C.-Y. Chan, and M. Tomizuka, "A Non-Conservatively Defensive Strategy for Urban Autonomous Driving," in *IEEE International Conference on Intelligent Transportation Systems*, Rio de Janeiro, Brazil, 2016, pp. 459–464.

[2] X. Qian, A. de La Fortelle, and F. Moutarde, "A Hierarchical Model Predictive Control Framework for On-road Formation Control of Autonomous Vehicles," in *IEEE Intelligent Vehicles Symposium*, Gothenburg, Sweden, 2016, pp. 376–381.

[3] J. Ziegler, P. Bender, T. Dang, and C. Stiller, "Trajectory planning for Bertha - A local, continuous method," in *IEEE Intelligent Vehicles Symposium*, Dearborn, Michigan, USA, 2014, pp. 450–457.

[4] Y. Gao, A. Gray, H. E. Tseng, and F. Borrelli, "A tube-based robust nonlinear predictive control approach to semiautonomous ground vehicles," *Vehicle System Dynamics*, vol. 52, no. 6, pp. 802–823, 2014.

[5] G. Williams, P. Drews, B. Goldfain, J. M. Rehg, and E. A. Theodorou, "Aggressive Driving with Model Predictive Path Integral Control," in *IEEE International Conference on Robotics and Automation*, Stockholm, Sweden, 2016, pp. 1433–1440.

[6] X. Qian, F. Altché, P. Bender, C. Stiller, and A. de La Fortelle, "Optimal Trajectory Planning for Autonomous Driving Integrating Logical Constraints : A MIQP Perspective," in *19th IEEE International Conference on Intelligent Transportation Systems*, Rio de Janeiro, Brazil, 2016, pp. 205–210.

[7] J. Liu, P. Jayakumar, J. L. Stein, and T. Ersal, "A multi-stage Optimization Formulations for MPC-based Obstacle Avoidance in Autonomous Vehicles using a LiDAR Sensor," in *ASME Dynamic Systems and Control Conference*, San Antonio, TX, USA, 2014, pp. 1–10.

[8] J. Kong, M. Pfeiffer, G. Schildbach, and F. Borrelli, "Kinematic and Dynamic Vehicle Models for Autonomous Driving Control Design," in *IEEE Intelligent Vehicles Symposium*, Seoul, Korea, 2015, pp. 1094–1099.

[9] T. Lozano-Perez, "Spatial Planning: A Configuration Space Approach," *IEEE Transactions on Computers*, vol. c-32, no. 2, pp. 108–120, 1983.

[10] J.-P. Laumond, "Feasible trajectories for mobile robots with kinematic and environment constraints," in *Intelligent Autonomous Systems, An International Conference*. Amsterdam, The Netherlands, The Netherlands: North-Holland Publishing Co., 1987, pp. 346–354.

[11] J. F. Canny, *The Complexity of Robot Motion Planning*. Cambridge, MA, USA: MIT Press, 1988.

[12] J. H. Reif, "Complexity of the mover's problem and generalizations," in *Proceedings of the 20th Annual Symposium on Foundations of Computer Science*. Washington, DC, USA: IEEE Computer Society, 1979, pp. 421–427.

[13] C. Katrakazas, M. Quddus, W.-H. Chen, and L. Deka, "Real-time motion planning methods for autonomous on-road driving: State-of-the-art and future research directions," *Transportation Research Part C: Emerging Technologies*, vol. 60, pp. 416–442, 2015.

[14] B. Paden, M. Cáp, S. Z. Yong, D. Yershov, and E. Frazzoli, "A Survey of Motion Planning and Control Techniques for Self-driving Urban Vehicles," *IEEE Transactions on Intelligent Vehicles*, vol. 1, no. 1, pp. 33–55, 2016.

[15] L. E. Dubins, "On Curves of Minimal Length with a Constraint on Average Curvature , and with Prescribed Initial and Terminal Positions and Tangents," *American Journal of Mathematics*, vol. 79, no. 3, pp. 497–516, 1957.

[16] J. Reeds and L. Shepp, "Optimal paths for a car that goes both forwards and backwards," *Pacific Journal of Mathematics*, vol. 145, no. 2, pp. 367–393, 1990.

[17] Y. Kuwata, S. Karaman, J. Teo, E. Frazzoli, J. P. How, and G. Fiore, "Real-Time Motion Planning With Applications to Autonomous Urban Driving," *IEEE Transactions on Control Systems Technology*, vol. 17, no. 5, pp. 1105–1118, 2009.

[18] V. Cardoso, J. Oliveira, T. Teixeira, C. Badue, F. Mutz, T. Oliveira-Santos, L. Veronese, and A. F. De Souza, "A Model-Predictive Motion Planner for the IARA Autonomous Car," *arXiv preprint arXiv:1611.04552*, nov 2016.

[19] M. A. Abbas, R. Milman, and J. M. Eklund, "Obstacle Avoidance in Real Time with Nonlinear Model Predictive Control of Autonomous Vehicles," in *IEEE Canadian Conference on Electrical and Computer Engineering*, 2014, pp. 1–6.

[20] R. Rajamani, *Vehicle Dynamics and Control*. Springer, 2012.

[21] C. Samson, "Control of Chained Systems Application to Path Following and Time-Varying Point-Stabilization of Mobile Robots," *IEEE Transactions on Automatic Control*, vol. 40, no. 1, pp. 64–77, 1995.

[22] R. C. Coulter, *Implementation of the Pure Pursuit Path Tracking Algorithm*. Carnegie Mellon University, 1992.

[23] M. Fliess, J. Lévine, P. Martin, and P. Rouchon, "Flatness and defect of non-linear systems: introductory theory and examples," *International journal of control*, vol. 61, no. 6, pp. 1327–1361, 1995.

[24] L. Menhour, B. d'Andréa Novel, M. Fliess, and H. Mounier, "Coupled nonlinear vehicle control: Flatness-based setting with algebraic estimation techniques," *Control Engineering Practice*, vol. 22, no. 1, pp. 135–146, 2013.

[25] P. Falcone, F. Borrelli, J. Asgari, H. E. Tseng, and D. Hrovat, "Predictive active steering control for autonomous vehicle systems," *IEEE Transactions on Control Systems Technology*, vol. 15, no. 3, pp. 566–580, 2007.

[26] P. Falcone, M. Tufo, F. Borrelli, J. Asgari, and H. Tseng, "A linear time varying model predictive control approach to the integrated vehicle dynamics control problem in autonomous systems," in *46th IEEE Conference on Decision and Control*, New Orleans, LA, USA, 2007, pp. 2980–2985.

[27] Y. Gao, T. Lin, F. Borrelli, E. Tseng, and D. Hrovat, "Predictive Control of Autonomous Ground Vehicles With Obstacle Avoidance on Slippery Roads," *ASME Conference Proceedings*, vol. 2010, pp. 265–272, 2010.

[28] K. J. Astrom and T. Hagglund, *PID Controllers: Theory, Design, and Tuning*. Instrument Society of America: Research Triangle Park, 1995.

[29] M. Fliess and C. Join, "Model-free control," *International Journal of Control*, vol. 86, no. 12, pp. 2228–2252, 2013.

[30] H. B. Pacejka, *Tyre and Vehicle Dynamics*. Butterworth-Heinemann, 2002.